# Direct Visualization of a Gold Nanoparticle Electron Trapping Effect

Oscar Bentley Jerdmyr Williams,[¶] Khabiboulakh Katsiev,[¶] Byeongjin Baek, George Harrison, Geoff Thornton,* and Hicham Idriss*

**ABSTRACT:** A new atomic scale anisotropy in the photoreaction of surface carboxylates on rutile $TiO_2(110)$ induced by gold clusters is found. STM and DFT+U are used to study this phenomenon by monitoring the photoreaction of a prototype hole scavenger molecule, benzoic acid, over stoichiometric (s) s $TiO_2$, $Au_9$/s $TiO_2$, and reduced (r) $Au_9$/r $TiO_2$. STM results show that benzoic acid adsorption displaces a large fraction of Au clusters from the terraces toward their edges. DFT calculations explain that $Au_9$ clusters on stoichiometric $TiO_2$ are distorted by benzoic acid adsorption. The influence of sub monolayers of Au on the UV/visible photoreaction of benzoic acid was explored at room temperature, with adsorbate depletion taken as a measure of activity. The empty sites, observed upon photoexcitation, occurred in elongated chains (2 to 6 molecules long) in the [110] and [001] directions. A roughly 3 fold higher depletion rate is observed in the [001] direction. This is linked to the anisotropic conduction of excited electrons along [001], with subsequent trapping by Au clusters leaving a higher concentration of holes and thus an increased decomposition rate. To our knowledge this is the first time that atomic scale directionality of a chemical reaction is reported upon photoexcitation of the semiconductor.

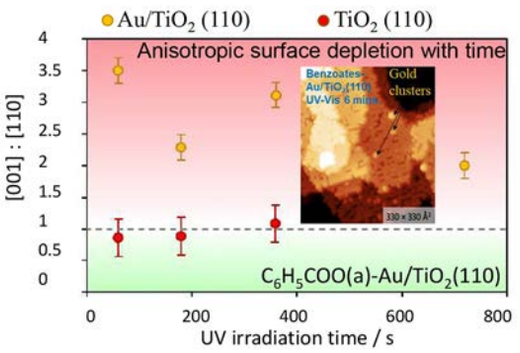


## 1. INTRODUCTION

Global environmental concerns have given rise to a pressing demand for clean, sustainable sources of energy. The photocatalytic production of hydrogen via water splitting is one of the most promising technologies to achieve this. Despite decades of work on different photocatalytic systems employing a variety of technical concepts, using sunlight to attain pure water splitting to molecular hydrogen and oxygen remains elusive.[1] This is due to the high level of complexity of the photocatalytic systems, wherein knowledge needs to be drawn from several scientific domains. To design a photo catalytic system with both long term stability and high photocatalytic rates, a profound knowledge of photophysics, energy transfer and kinetics of surface reactions, and material science is required. One approach to tackle this problem is to conduct model photocatalytic studies in order to understand the fundamental steps of the process.

Following the pioneering work of Fujishima and Honda,[2] there has been significant interest in $TiO_2$ based photo catalysis, both to understand the fundamental science and to harness this effect for industrial applications. Extensive research has been carried out on various forms of metal deposited on titania powder and single crystals. One of the most studied and understood surfaces of an oxide semiconductor is the rutile $TiO_2(110)$, making it an ideal system to conduct model catalyst studies.

Reactions of oxygen containing organic molecules on photoexcited $TiO_2$ proceed through a hole scavenging mechanism in which, upon photoexcitation, electrons are transferred from the valence band (VB) to the conduction band (CB) of the semiconductor, leading to an electron−hole pair "exciton". The electron−hole separation creates a hole (electron) oxidant (reductant). On $TiO_2$ and other oxide semiconductors with similar energy gaps, the excited electrons in the conduction band can then be transferred to surface adsorbed $O_2$, forming $O_2^-$ (oxygen anion radicals), which decreases the recombinative electron (e)−hole (h) rate.[3−5] For example, in the photo oxidation of ethanol/ethoxides ($CH_3CH_2O$ (a)) on $TiO_2(110)$ the first step involves the abstraction of a hydrogen atom (strictly $H^+ + 2e$) from the $\alpha$ carbon atom, which leads to $CH_3CHO$ desorption. The amount of acetaldehyde detected in the gas phase was found to increase with increasing $O_2$ partial pressure. A fraction of the acetaldehyde undergoes a further oxidation step and is converted, via carboxylate species, to $CO_2$.[6] Carboxylates were detected by noting their XPS C 1s signal upon UV light exposure in the presence of $O_2$.[7] This mechanism is also seen on powder catalysts by in situ and in operando IR spectroscopy, wherein the photo oxidation of primary and

secondary alcohols as well as ketones leads to the formation of carboxylate species.[8,9]

Carboxylic acids have been studied in detail on the surfaces of rutile $TiO_2(110)$,[10,11] (100),[12] and (011)[13,14] by many experimental and computational methods. Dissociative adsorp tion results in ordered structures with close to 0.5 monolayer (ML, which is defined as a fraction of the number density of $Ti_{5c}$ sites on an ideal planar surface, $5.2 \times 10^{14}$ Ti atoms $cm^{-2}$) saturation coverage on the (110) surface, with bidentate bonding of carboxylates to two Ti cations along the [001] direction. The ordered structures allow the study of both electronic and geometric effects and therefore provide unique systems to decouple these interconnected properties.

As for gold deposition, this has been studied in detail for $TiO_2(110)$, with a variety of nanoparticle shapes and sizes being observed.[15,16] Within the context of this work, we focus on Au clusters with diameters between 0.3 and 1 nm. We have also previously studied the photoreaction of ethanol/ethoxides on these clusters over $TiO_2(110)$.[17] Their effect was found to be similar to that of molecular oxygen, their high electron affinity trapping excited electrons and consequently promoting photocatalytic reactions. The adsorption energies of gold atoms and clusters on $TiO_2(110)$ have previously been computed and found to be dependent on the nature of the binding site in addition to the number of gold atoms per cluster. Values ranging from 0.5 to 3 eV per atom have been reported.[18,19] Au clusters have a key function in photoreaction. They heal most "ground state" $Ti^{3+}$ sites upon their deposition.[20] These $Ti^{3+}$ sites have been proposed to be hole traps during photoexcitation;[21] hence their depletion will increase the photocatalytic reaction rate. As a metal with a high work function, like Pt and Pd, Au nanoparticles trap excited electrons generated upon light excitation of a semiconductor such as $TiO_2$.[22] Au clusters and particles of finite sizes also have pronounced plasmon resonances, responding to light with cluster size dependent wavelengths in the visible region.[23] It has been found by using polarized excitation light that Au clusters on $TiO_2(110)$ terraces have a strong plasmon response perpendicular to the surface[24] extending over wavelengths from 300 to 600 nm. The gold plasmon oscillating frequency is typically in the $10^{15}$ $s^{-1}$ range, which is many orders of magnitude higher than the period of excited charge propagation in $TiO_2$ (typically in the ps to ns range).[25] For this reason, the electric field induced at the semiconductor interface decreases the e−h recombination rate. Hence Au clusters on $TiO_2(110)$ have at least three beneficial effects on its photoreaction: (1) They heal $Ti^{3+}$ upon deposition, (2) they trap excited electrons, and (3) their plasmon response can accelerate charge carrier propagation.

Anisotropy of charge diffusion has been recognized early on for rutile $TiO_2(110)$.[26,27] It was observed that the conductivity was 3−6 times higher along the [001] direction when compared to that along the [110] direction. It has also been observed that Ar ion sputtering causes anisotropy of Ti−O species along the [001] direction[28] irrespective of the azimuth of sputtering.

Among the most studied carboxylic acids over $TiO_2(110)$ single crystals is trimethyl acetic (TMA) acid under photon irradiation.[29,30] Like other carboxylic acids,[31,32] the presence of molecular oxygen enhances their photodecomposition. It was also found that deliberately reducing the surface of $TiO_2(110)$ was not beneficial for the reaction,[33] instead decreasing its yield. Reduced sites ($Ti^{3+}$) repel excited electrons, which in turn increases their recombination rate with holes.[35]

In this study, we have investigated the photoreaction of benzoic acid (BA) as a prototype hole scavenger organic molecule adsorbed on rutile $TiO_2(110)$. We used STM and DFT+U calculations to gain insights into the photocatalysis of BA on the s $TiO_2(110)$ and Au/r $TiO_2(110)$ surfaces, with gold predeposited at sub monolayer coverages (ca. 0.1 MLE).

## 2. EXPERIMENTAL DETAILS

Experiments were undertaken in a UHV system consisting of two chambers separated by a gate valve. The analysis chamber had a base pressure of $1 \times 10^{-10}$ mbar and houses a Specs Aarhus HT 150 variable temperature STM, a sputter gun, and an e beam heater for sample preparation. The auxiliary chamber had a base pressure of $5 \times 10^{-10}$ mbar and contains a precision leak valve for the dosing of benzoic acid. UV−visible light irradiation was conducted through a boron silicate UHV window in the auxiliary chamber using a Xenon Arc 300 W MAX 303 Asahi Spectra Xe lamp. The lamp delivered 690 mW $cm^{-2}$ over a range of wavelengths from 320 to 630 nm. This power output equates to a flux of around $1.64 \times 10^{18}$ photons $s^{-1}$ $cm^{-2}$ on the sample surface.

A rutile (110) single crystal (Matek) of dimensions $10 \times 5 \times 2$ $mm^3$ was used in this work. The crystal was held in place on a Ta sample plate using two spot welded Ta strips. In order to prepare the $TiO_2(110)(1 \times 1)$ surface under UHV conditions, cycles of $Ar^+$ sputtering (10−15 min, 1 keV, 5 $\mu$A, $P = 1 \times 10^{-5}$ mbar) and UHV annealing (10 min, 950 K) were carried out until a flat, contaminant free surface was seen, as verified by STM imaging. During preparation, the transparent rutile crystal turns a deep blue color, the surface having 3−10% ML bridging oxygen vacancies. The surface was considered clean once a minimal coverage of large contaminant species (roughly 0.005 ML or below) was visible using STM, with characteristic steps and a surface unit cell of $3 \times 6.5$ $Å^2$. The surface was subsequently hydroxylated through exposure to residual water present in the UHV chamber, resulting in a coverage of around 0.1 ML of bridging hydroxyls (within minutes at room temperature). This h $TiO_2(110)$ surface was selected for investigation because it is a stable surface and probably the most representative of the (110) facets seen in polycrystalline materials. Au nucleation and cluster growth have been investigated previously.[36,37] Calibration of the three STM piezos ($x$, $y$, and $z$ piezos) was carried out using the size of the rutile surface unit cell and the known step height of 3.25 Å.

The STM tip was fabricated by electrochemical etching of a 0.2 mm diameter tungsten wire. Prior to measurements, the tip was conditioned using repetitive pulses of +5 V sample bias until atomic resolution was attained. Benzoic acid (99.9%, Sigma Aldrich) was contained in a glass vial attached to a gas manifold, and this was dosed onto the sample by backfilling the auxiliary UHV chamber using a high precision leak valve. The purification of benzoic acid was found to be a crucial step. The cleanest conditions were obtained upon pumping the vial and acid for 48 h at room temperature, using a turbomolecular pump. Because it is solid at room temperature, to build up sufficient pressure in the gas line, a baking tape was used to heat the gas manifold and leak valve. The solid acid was sublimed by submerging the vial in a bath of hot water (~360 K), the baking tape being employed to maintain the acid at temperature (~350 K) in the line in order to avoid condensation on its interior wall. The purity of the gas was monitored during dosing through RGA mass spectrometry. Exposures of benzoic acid in this body of work are quoted in Langmuir (L) ($1\ L = 1.33 \times 10^{-6}$ mbar s), where the uncompensated chamber pressure, connected to the STM chamber via the gate valve, was roughly at $4 \times 10^{-9}$ mbar. This avoided contaminating the STM chamber.

Gold was deposited onto the sample surface under UHV at room temperature, through physical vapor deposition of an ultra high purity gold wire (Goodfellow) wrapped around a filament that was resistively heated. The sizes of Au clusters were monitored over time at room temperature, and no size or morphological changes were

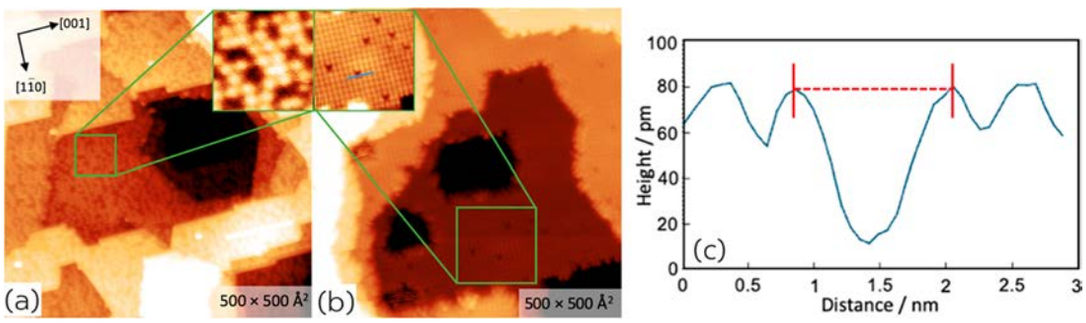


**Figure 1.** STM images of $TiO_2$ rutile (110) surface before and after exposure to 10 L of benzoic acid: (a) large area image of clean rutile (110) ($V_s$ = +2.09 V, 0.03 nA). Inset of 50 Å × 50 Å (see SI Figure S3 for more details). (b) Large area image of the near pristine benzoate monolayer formed on the clean $TiO_2$ rutile (110) (+1.90 V, 0.03 nA). Inset of 100 Å × 100 Å highlights the point (adsorbate) defect vacancies, seen as dark spots on the overlayer. This overlayer gives a coverage of 0.48 ML. (c) Line profile taken from the STM image, as depicted by the blue line in the inset of (b), across four benzoate molecules and a benzoate vacancy showing the (2 × 1) spacing of 12 Å as measured by the red dotted line between two adjacent benzoate molecules and an apparent height of the molecules of ∼70 pm.

observed. The gold coverage is defined as a fraction of the coverage of gold atoms on the Au(111) surface (MLE), and this was measured using STM with a full monolayer defined as $1.387 \times 10^{15}$ atoms $cm^{-2}$.

## 3. COMPUTATIONAL DETAILS

Density functional theory (DFT) simulations were performed using the Vienna Ab initio Simulation Package (VASP).[38−40] The projector augmented wave (PAW) method and generalized gradient approximation (GGA) with Perdew−Burke−Ernzerhoff (PBE) in combination with BEEF vdW functionals solved the Kohn−Sham equations.[41,42] The atomic simulations environment (ASE) was used to create a bulk $TiO_2$ and slabs.[43] All surface calculations had a cutoff energy of 400 eV for the plane wave basis set. The on site Coulombic interaction of the localized Ti 3d states was corrected by the Dudarev approach using the previously reported $U_{eff}$ value of 4.2 eV.[44,45] The Brillouin zone with Monkhorst−Pack meshes was sampled with (13 × 13 × 15) for bulk calculations and (4 × 4 × 1) for surface relaxations.[46] The optimized lattice constants for rutile $TiO_2$ are $a$ = 4.705 Å, $c/a$ = 0.641, which are in good agreement with experimental values.[47] The optimized bulk structure was used to build a periodically repeated four layers of stoichiometric (5 × 3) $TiO_2$(110), s $TiO_2$(110), of which the top two layers were fully relaxed, while the bottom two layers were fixed at their bulk positions. To minimize the surface interactions, a vacuum space of 20 Å over the slab was added. Nine gold atom ($Au_9$) clusters were modeled on the reduced (5 × 3) $TiO_2$ surface, r $TiO_2$(110) and (5 × 3) s $TiO_2$(110) surfaces. The cluster size was dictated by the needed stability on the surface (upon relaxation) and to be close to the experimental value. On the r $TiO_2$(110), one bridge oxygen atom was removed to anchor the Au cluster. Several configurations of Au clusters were explored to find the most stable Au structure on slabs; the Au cluster was distorted as it interacted with neighbor bridge oxygen atoms and the underneath vacancy. An energy minimization of four Au atoms (initially 3D Au cluster) resulted in the formation of a 2D island. Clusters made of nine Au atoms maintained the 3D configuration after minimization (hcp crystal structure). The most stable configuration had a slightly distorted equilateral triangle, composed of six atoms, as a base, with a side of ca. 7.2 Å, and three on top. The nine configurations of the $Au_9$ clusters studied on s $TiO_2$ and 13 configurations on r $TiO_2$ are included in the Supporting Information (see SI Figure S1). Surface relaxations were conducted with a force convergence of 0.05 eV/Å. The binding energies ($E_b$) were calculated as given by

$$E_b(i) = E_{i@s} - E_s - E_g \quad (1)$$

where $E_{i@s}$ is the total energy of the surface with adsorbate "$i$" (benzoic acid or benzoate), $E_s$ is the energy of clean surfaces (s $TiO_2$(110), $Au_9$/s $TiO_2$(110), or $Au_9$/r $TiO_2$(110)), and $E_g$ is the total energy of gas phase species (hydrogen and benzoic acid). Relaxations of gas phase species (benzoic acid and hydrogen) were performed in a 20 × 20 × 20 $Å^3$ box using only Γ point integration with a force convergence of 0.01 eV/Å. Transition states were located with the climbing image nudged elastic band (cNEB) method by using five or six images.[48] To study the electronic structure, the density of states (DOS) was calculated using a $k$ point of (8 × 8 × 1) for integrating the Brillouin zone. The surface coverage is with respect to surface $Ti^{4+}_{5c}$.

## 4. RESULTS AND DISCUSSION

**4.1. Gold and Benzoic Acid Adsorption on Rutile $TiO_2$(110)-(1 × 1).** Stoichiometric rutile $TiO_2$(110) displays a (1 × 1) surface termination with monatomic steps of 3.25 Å and terraces of around 150 Å size. As seen in Figure 1(a), at high resolution the STM image contrast is dominated by bright features of apparent height 0.8 Å and aligned in rows along the [001] direction separated by 3 Å. These bright features are bridging hydroxyls ($HO_{br}$) that sit at the position of bridging oxygen atoms ($O_{br}$).[49] The coverage of hydroxyls is calculated to be ca. 0.1 ML, where a monolayer is defined as one adsorbate per primitive surface unit cell (a density of approximately $5.2 \times 10^{14}$ $cm^{-2}$). Therefore, the surface can be considered to be partially hydrated. In atomically resolved STM images, when imaging empty states (under a positive sample bias) with a lower density of $OH_{br}$ sites, bright rows of $Ti_{5c}$ cations run along the [001] direction, alternating with darker rows of $O_{br}$ surface ions.[50] Rutile $TiO_2$(110) surfaces exposed to benzoic acid contain bright protrusions in empty states STM, with different structured overlayers depending on the deposition method. It forms a nearly perfect (2 × 1) benzoate monolayer with few defects (approximately 0.04 ML) when benzoic acid deposited from the gas phase. This is in contrast to the (2 × 2) dimer benzoate arrangements (or bilayered), when benzoic acid deposited from liquid phase.[51,52]

The surface exposed to benzoic acid (10 L) formed a (2 × 1) benzoate overlayer. This is consistent with a dissociative bidentate binding geometry of benzoate bridging two neighboring $Ti_{5c}$ ions in the [001] direction, as seen in the previous work.[53] The corresponding image can be seen in Figure 1(b), with the inset highlighting the dark point defects or molecular vacancies. A vacancy in Figure 1(b) is defined as an empty adsorption site that is composed of two $Ti^{4+}$ cations along the [001] direction. In STM images, a coverage of 0.48 ML is observed. The (2 × 1) spacing is evidenced by the line profile in Figure 1(c). The line profile includes a molecular vacancy as measured from a single isolated vacancy on an atomic terrace, giving an apparent height of ∼70 pm (0.7 Å) at a sample bias of +2.1 V, which is roughly 3 times smaller than that reported in the literature.[55] This discrepancy is likely due to tip convolution effects, and the 12 Å width of the vacancy, observed in Figure 1(c), is similar to that previously reported. A boundary between (2 × 1) domains is occasionally seen on the monolayer, whereby there is a dislocation of one single lattice spacing between the two regions. This phenomenon was also observed in other studies of small carboxylic acids deposited on the $TiO_2$(110) surface.[54] Horizontal streaks were frequently seen when imaging the benzoate monolayer, indicative of tip−surface interactions or structural change in the monolayer. This may involve tip induced benzoate diffusion across the surface. We evidence this when the same area of the surface is imaged consecutively to create an STM movie with around 120 s between each frame. The comparison between frames helps to map out the position of all molecular vacancies in the initial frame and then compare them to the next frame, highlighting those vacancies that have stayed immobile, those that have disappeared between one frame and another, and "new" vacancies that appear in the second frame. It was often found that the vacancy sites that disappeared and the new vacancy sites that appeared are paired, suggesting a diffusion of molecules between the two. This gives a proportion of vacancies, or molecules, that are mobile, determined to be at an average of 8% on the benzoic acid dosed $TiO_2$(110) surface. The proportion of mobile molecules can give insight into the diffusion dynamics on the surface, and an example of two frames analyzed in this way is shown in SI Figure S2.

To understand the thermodynamics and adsorption configurations of benzoic acid and benzoate, we performed DFT+U calculations on both s $TiO_2$(110) and r $TiO_2$(110) surfaces. The computed values including binding energies ($E_b$) and energy barriers ($E_a$) are tabulated in Table 1. Two adsorption configurations of benzoic acid, with the benzene ring parallel and perpendicular to the [001] direction, were initially studied. Figure 2(a) shows its most stable configuration, in which the benzene ring is perpendicularly orientated in the [001] direction. This structure has an interaction between the proton of the hydroxyl group ($HO_m$, "m" denotes molecule) of the adsorbed benzoic acid and the $O_{br}$ site. The distance between the $O_{br}$ and the $HO_m$ is 1.47 Å. The length of the C═O bond in direct interaction with $Ti^{4+}_{5c}$ is equal to 1.27 Å (vs 1.22 Å in the gas phase benzoic acid). The adsorption of benzoic acid is thermodynamically stable with a binding energy of −1.59 eV. This adsorbed benzoic acid undergoes OH bond scission with a barrier of 0.38 eV, forming surface benzoate and $HO_{br}$; see Figure 2(b). The computed binding energy of the dissociated benzoate and $HO_{br}$ is thermodynamically more downhill by −0.84 eV than the binding energy of benzoic acid. With these energetics, benzoic acid is likely to convert into benzoate on the $TiO_2$(110) surface, as seen before,[11] with an adsorption energy of −2.43 eV at a coverage of 0.06 ML.

**Table 1. Calculated Energies Associated with Adsorption, Diffusion, and O−H Bond Scission**[a]

| reaction | surface | $\Delta E$, $E_b$ [eV] | $E_a$ [eV] | distance [Å] |
|---|---|---|---|---|
| $BA_{(g)} + Ti_{5c} \rightarrow BA\text{-}Ti_{5c}$ | s-$TiO_2$(110) | 1.59 | | |
| $BA\text{-}Ti_{5c} + O_{br} \rightarrow B\text{-}Ti_{5c} + HO_{br}$ | s-$TiO_2$(110) | 0.84 | 0.38 | $d^{BA-Ti}_{O-C_{5c}} = 1.27$, $d^{BA\ Ti}_{C-O_{5c}} = 1.30$, $d^{BA-Ti}_{O-H_{5c}} = 1.04$ |
| $BA_{(g)} + Ti_{5c} \rightarrow BA\text{-}Ti_{5c}$ | $Au_9$/s-$TiO_2$(110) | 1.62 | | $d^{BA-Ti}_{O-H_{5c}} = 1.57$ |
| $BA_{(g)} + Ti_{5c} \rightarrow BA\text{-}Ti_{5c}$ | $Au_9$/r-$TiO_2$(110) | 1.68 | | $d^{BA-Ti}_{O-H_{5c}} = 1.02$ |
| $BA\text{-}Ti_{5c} + O_{br} \rightarrow B\text{-}Ti_{5c} + HO_{br}$ | $Au_9$/r-$TiO_2$(110) | 0.83 | 0.06 | $d^{BA-Ti}_{O-C_{5c}} = 1.26$, $d^{BA-Ti}_{C-O_{5c}} = 1.31$, $d^{BA-Ti}_{O-H_{5c}} = 1.02$ |
| $B\text{-}Ti_{5c} \rightarrow B\text{-}Ti_{5c}$ (diffusion) | s-$TiO_2$(110) | 0.03 | 1.46 | |
| $B\text{-}Ti_{5c} \rightarrow B\text{-}Ti_{5c}$ (diffusion) | $1HO_{br}$ + s-$TiO_2$(110) | 0.01 | 1.51 | $d^{l\,B-Ti}_{O-HO_{brSC}} = 2.65$ |
| $B\text{-}Ti_{5c} \rightarrow B\text{-}Ti_{5c}$ (diffusion) | $2HO_{br}$ + s-$TiO_2$(110) | 0.05 | 1.56 | $d^{l\,B-Ti}_{O-HO_{brSC}} = 2.67$, $d^{r\,B-Ti}_{O-HO_{brSC}} = 2.62$ |
| $B\text{-}Ti_{5c} \rightarrow B\text{-}Ti_{5c}$ (diffusion) | $3HO_{br}$ + s-$TiO_2$(110) | 0.01 | 1.59 | $d^{l\,B-Ti}_{O-HO_{brSC}} = 3.71$, $d^{r\,B-Ti}_{O-HO_{brSC}} = 2.48$ |

[a]BA and B stand for benzoic acid ($C_6H_5COOH$) and benzoates ($C_6H_5COO(a)$), respectively. $Ti_{5c}$ and $O_{br}$ indicate the binding site of the five coordinated Ti and bridge oxygen atoms. The $O^l$ and $O^r$ correspond to the left and right oxygen atoms in the −COO− group of benzoate. The subscript (g) stands for gas phase. The $E_b$, $\Delta E$, and $E_a$ are binding energy, energy difference between initial and final states, and activation energy, respectively. The nomenclature of bond length consists of adsorbate binding sites and corresponding bond. For example, $d^{BA-Ti}_{O-C_{5C}}$) indicates the bond length of O−C in BA that adsorbs on the $Ti_{5C}$ site.

Figure 3 presents diffusion barriers of benzoate along the [001] direction with respect to the number of adjacent $HO_{br}$ sites. The diffusion of benzoate is kinetically limited with an average barrier of 1.52 eV due to the strong interaction between $Ti^{4+}_{5c}$ sites and oxygen atoms of the −COO− group in benzoate. During the diffusion, an intermediate species is formed that has 7 fold coordinated $Ti^{4+}$ cations to the two oxygen atoms of the carboxylic function. This can be rationalized by the delocalization of one electron along the −COO− group. The large distance between the Ti atoms and the two oxygen atoms (2.19 Å) is most likely a consequence of the high coordination number of the Ti cation. The presence of surface hydroxyls increases the diffusion barrier, and the effect seems to be additive up to the second hydroxyl (Figure 3); the presence of three adjacent $HO_{br}$ increases the diffusion barrier by 0.12 eV compared to the diffusion barrier in the absence of $HO_{br}$. This can be attributed to hydrogen bonding between $HO_{br}$ sites and the carboxylate group and to the associated twisting of the ring during the diffusion along the [001] direction.

A room temperature STM image of gold deposited on s $TiO_2$(110) is shown in Figure 4(a), which corresponds to a coverage of around 0.12 ML. Sub nanometer hemispherical features are identified as gold clusters, and these are formed at room temperature through surface diffusion and nucleation.[55] Before dosing the surface with benzoic acid, the majority

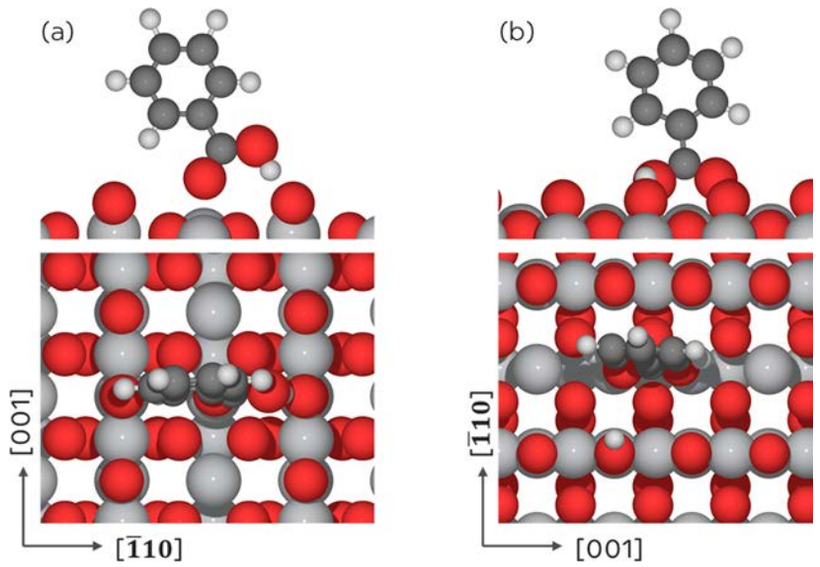


**Figure 2.** Side and top views of molecular (a) and dissociative (b) adsorption of benzoic acid over stoichiometric rutile $TiO_2$(110). The surface coverage is around 0.06 ML. Color code: carbon, dark gray; oxygen, red; hydrogen, white; titanium, gray.

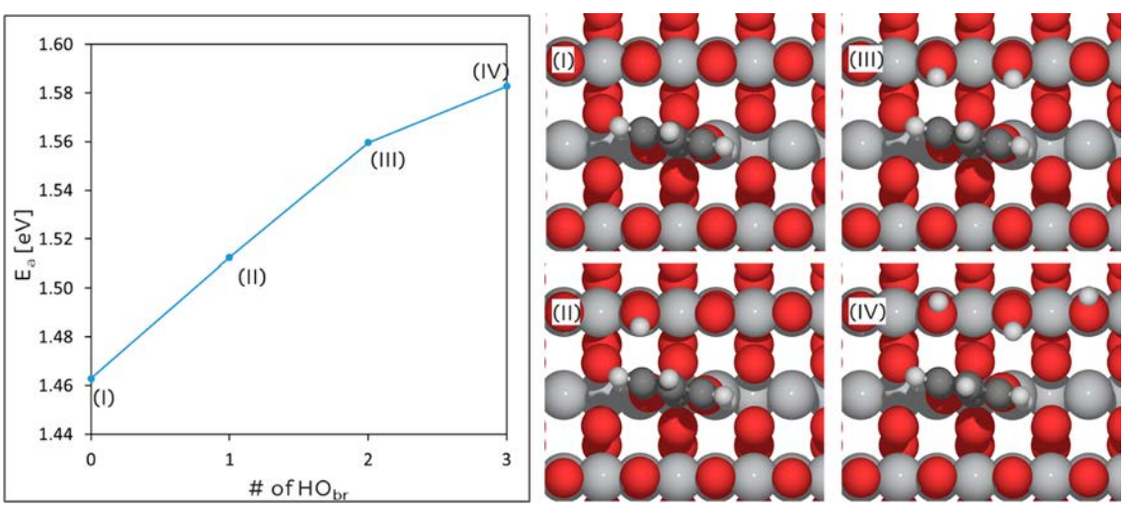


**Figure 3.** Calculated diffusion barriers for an isolated benzoate species along the [001] direction on the s $TiO_2$(110) surface with respect to the number of $HO_{br}$. The roman numeral corresponds to each final state of benzoate diffusion: (I) benzoate on the $TiO_2$(110), (II) benzoate on the $HO_{br}$/s $TiO_2$(110), (III) benzoate on the $2HO_{br}$/s $TiO_2$(110), and (IV) benzoate on the $3HO_{br}$/s $TiO_2$(110). Color code: carbon, dark gray; oxygen, red; hydrogen, white; titanium, gray.

(>90%) of clusters had a diameter below 1 nm, as evidenced by the height−width plot shown in blue in Figure 4(c). This is similar to what we have observed before on the same surface using the same dosing technique and setup[17] (more information can be found in Tables S1 and S2 of ref 17; the mean diameter of Au particles was found to be between 7 and 9 Å, from which the number of atoms per cluster was extracted and found to be between 11 and 15). The line profile of a representative gold species on the surface is indicated by the blue line in Figure 4(a), with the height profile as shown in the inset of Figure 4(c). The Au/$TiO_2$(110) surface was successively exposed to benzoic acid (10 L), and a (2 × 1) benzoate overlayer was still formed as described above on the clean surface and shown in Figure 4(b). After dosing benzoic acid, the gold sinters together and forms larger clusters. This change in the size of the gold species is demonstrated through the difference in the height distributions before and after dosing, the latter being plotted in red in Figure 4(c). Further, this is also highlighted by the inset line profiles, with the much larger profile in red showing the typical size after exposure to benzoic acid. The height of a gold cluster nucleated at a step edge is taken to be the average of the height of the gold from the lower terrace and the height from the upper. This indicates that the adsorption of benzoic acid molecules provides enough energy for Au atoms to overcome the energetic barrier of their diffusion, until they sinter to form larger clusters with higher adsorption energies. In other words, it seems that the adsorption energy of about −2.4 eV per benzoic acid molecule is enough to overcome the energy barrier for Au cluster diffusion within the investigated size range ($E_{a(diffusion)}$ = ca. 0.5 eV for $Au_9$; see Section 4.2).

To further understand the characteristics of Au clusters on $TiO_2$(110) and consequently their effect on photoreactions, DFT calculations for a $Au_9$ cluster on both s and r $TiO_2$ surfaces were performed. We have opted to use a gold cluster of nine atoms after many trials in which we wanted to have a

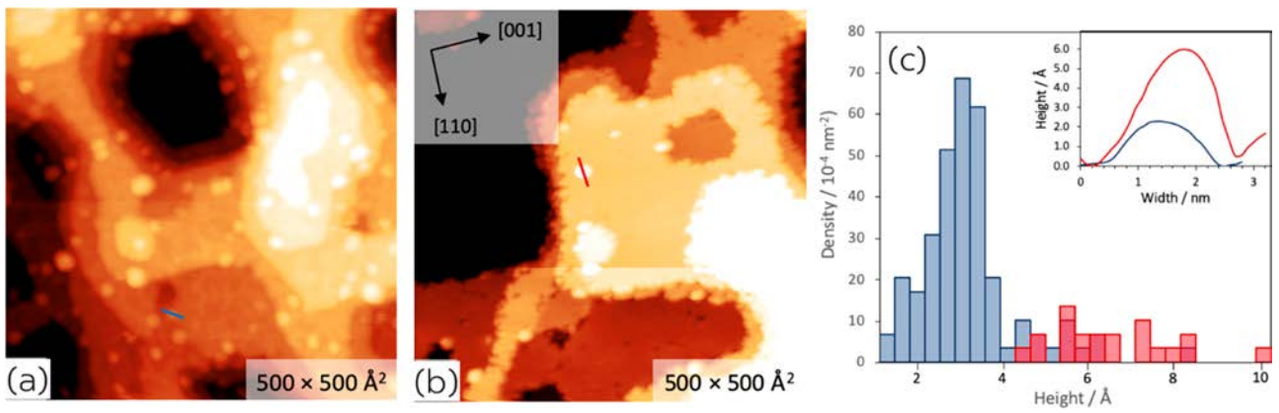


**Figure 4.** Large scale STM images of the Au loaded $TiO_2$ rutile (110) surface before and after dosing benzoic acid: (a) A typical rutile (110) surface following gold deposition of 0.12 ML, taken at a tip voltage of +2.2 V, 0.03 nA. (b) The same surface after dosing benzoic acid. (c) Height distribution of gold species on the surface before benzoic acid is dosed, in blue, and after dosing in red. Inset shows corresponding line profiles of the average gold species before (blue) and after (red) benzoic acid dosage, to highlight the difference in sizes.

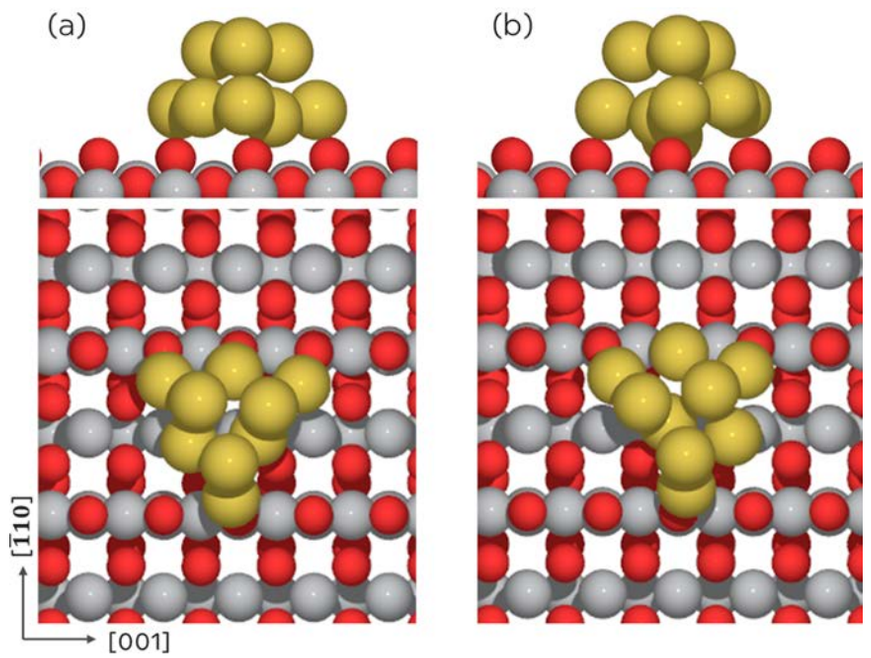


**Figure 5.** Top and side views of the relaxed $Au_9$ clusters on (a) s $TiO_2$ and on (b) r $TiO_2$. Color code: oxygen, red; titanium, gray; and gold, yellow.

stable cluster with at least two layers and with a size comparable to the one observed experimentally. The number of Au atoms and their shape are similar to those adopted in previous studies of Au on $TiO_2$.[56,57] Figure 5 shows the relaxed geometries calculated for $Au_9$ clusters deposited on s and r $TiO_2(110)$. All studied configurations of $Au_9$ after relaxation are given in SI Figure S1, and the most stable configurations are chosen for further analysis. The computed adsorption energies of the cluster are −2.15 eV on s $TiO_2(110)$ and −2.85 eV on r $TiO_2(110)$; these values are referenced to the gas phase $Au_9$ cluster. On s $TiO_2(110)$, the $Au_9$ cluster adsorption transfers a charge to $TiO_2$ with a total Bader charge of +0.65*e*. On the other hand, on the reduced surface, charge transfer occurs from r $TiO_2(110)$ to the $Au_9$ cluster, which consequently shows an average Bader charge of −0.21*e*. Recent modeling of one, two, and three gold atoms on $TiO_2(110)$ found that for $Au_1$ and $Au_3$ electron transfer occurs from Au to $TiO_2$ on the stoichiometric surface and vice versa on the reduced surface.[58] The local Bader charge of the $Au_9$ cluster on r $TiO_2(110)$ depends on their location. For instance, the excess charge is preferentially distributed on Au atoms away from the interface with r $TiO_2$; see SI Figure S4 for the local charge distribution of the Au cluster on the r $TiO_2$. One Au atom on r $TiO_2(110)$ strongly interacts with the bridge vacancy site, giving the Au cluster a distorted pyramidal shape (on s $TiO_2(110)$, the $Au_9$ cluster forms a truncated pyramidal structure). As previously reported,[59] the $O_{br}$ sites interact with Au atoms, resulting in an average distance of 2.29 Å on the s $TiO_2(110)$ and 2.25 Å on r $TiO_2(110)$. The shorter bond length is also a reflection of a stronger binding of Au clusters to r $TiO_2(110)$ than to s $TiO_2(110)$.

The adsorption of benzoic acid was further studied on both s and r $TiO_2(110)$ (see Figure 6). Benzoic acid adsorbs on the $Ti_{5c}^{4+}$ site with a binding energy of −1.62 eV on the $Au_9$/s $TiO_2$

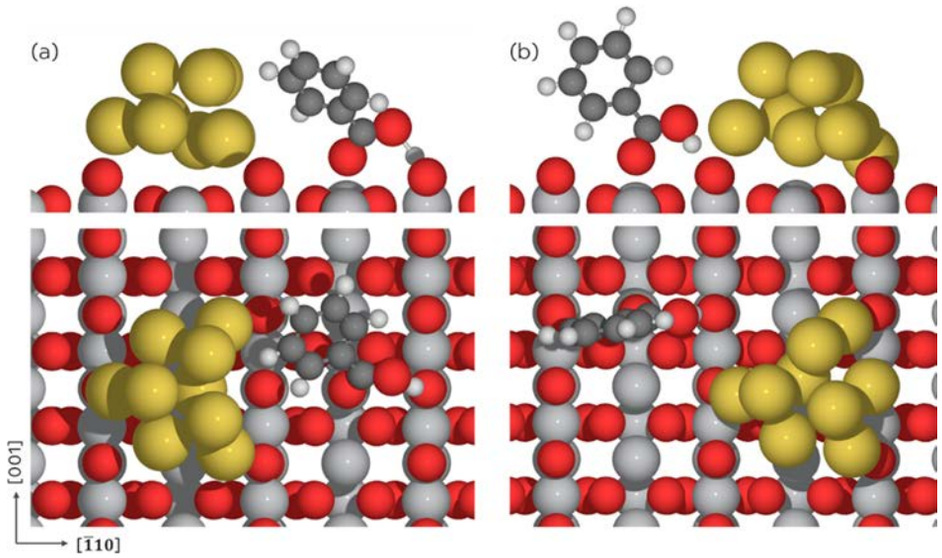


**Figure 6.** Side and top views of benzoic acid adsorption (with a coverage of ca. 0.07 ML) on (a) $Au_9$/s $TiO_2$(110) and (b) $Au_9$/r $TiO_2$(110). Color code: carbon, dark gray; oxygen, red; hydrogen, white; titanium, gray; gold, yellow.

and −1.68 eV on the $Au_9$/r $TiO_2$. The presence of a Au cluster facilitates the deprotonation of benzoic acid. As shown in Figure 6(a), the O−H bond appears to be located at a metastable point as its bond length stretches to 1.57 Å by interacting with the $O_{br}$ site (forming hydrogen bonding). On Au/r $TiO_2$(110), this meta state of benzoic acid was not observed, as shown in Figure 6(b). Instead, the OH group of benzoic acid interacts with the neighboring $O_{br}$ site by the Au cluster. The estimated barrier of O−H bond scission on $Au_9$/r $TiO_2$ is 0.06 eV (virtually barrierless), which is much lower than on stoichiometric $TiO_2$ (0.38 eV). This might be a result of the charge transfer from r $TiO_2$ to the Au cluster, as observed in this work, resulting in a change of electronic structure near the Au cluster, as reported elsewhere.[60,61] On Au/s $TiO_2$, the adsorption of benzoic acid (before its dissociation) deforms the Au cluster considerably, while on r $TiO_2$, the Au atoms remain in their initial positions. To further verify this, we recomputed the system, but in this case took the final adsorption configuration of benzoic acid on the stoichiometric surface shown in Figure 6(a) and used it as the starting configuration for the Au cluster on the reduced surface. Negligible deformation of the Au cluster occurred (see SI Figure S5). It is to be noted that the aromatic ring points toward the Au cluster on the stoichiometric $TiO_2$, but away from the Au cluster on the r $TiO_2$, and this is probably the cause for distortion. This might be related to an electrostatic interaction where the aromatic ring (high electron density) interacts with the positively charged Au cluster on the stoichiometric $TiO_2$, but is repelled by the negatively charged Au cluster on r $TiO_2$. This interaction therefore contributes to the Au cluster deformation, which leads to the diffusion of the Au cluster. To analyze this further, we have calculated the projected density of states (pDOS) for the C atom of benzoic acid and the Au shown in Figure 6(a). Overlaps between C(p) and Au(d) located at around −3 eV indicate a $\pi$ type interaction between the Au cluster and the benzene ring of benzoic acid (see SI Figure S6).

The diffusion barrier for the $Au_9$ cluster along the [001] direction was calculated for s $TiO_2$(110). We found that a barrier of 0.48 eV is required, which is much lower than the energy gained by the adsorption of benzoic acid. Li et al. reported[62] a similar barrier of 0.42 eV for Au diffusion along the [001] direction. It has been also reported[63] that Au atoms on s $TiO_2$ have a preference to diffuse along [001]. Having calculated the diffusion barrier for $Au_9$, we postulate that the energy gained by the adsorption of benzoic acid provides the necessary energy for the Au cluster to diffuse to the step edges shown in the STM images (see Figure 4).

**4.2. Effect of Gold on the Photodynamics of Benzoate on $TiO_2$(110).** Empty benzoate sites are formed when the (2 × 1) benzoate overlayer is exposed to UV−vis light, appearing as dark patches on the (2 × 1) monolayer. This is in contrast to a previous STM study of benzoic acid adsorbed onto the $TiO_2$(110) surface that reported this surface to be stable under UV irradiation even after several hours.[64] The coverage of benzoate after irradiation is used as a measure of the rate of the photoinduced surface reaction, which is likely to involve oxidation of the benzoate species.

After irradiation, an interesting phenomenon is observed in the benzoate layer, whereby "chains" of consecutive empty benzoate sites are preferentially aligned either perpendicular to the $Ti_{sc}$ rows (in the [110]) or parallel to the rows (along [001]). Examples of these chains are presented in Figure 7(a) in the absence of a Au cluster and (b) in the presence of Au. It should be noted that both images were selected to display similar coverages of benzoate for a direct comparison. More information regarding the time effect is given in SI Figure S7. We have not monitored the reaction products because the configuration of the STM setup does not allow for excitation and gas phase product monitoring at the same time. The reaction is most likely akin to other hole driven reactions of carboxylic acids (yielding $CO_2$ and a hydrocarbon from the chain). In this case, in its simplest expression it can be written as $C_6H_5$ COO(a) + OH(a) + (h + e) → $C_6H_6$ + $CO_2$ ($\Delta G^\circ$ = 28 kJ $mol^{-1}$, $E^\circ_{ox}$ = −0.14 V (versus SHE: standard hydrogen electrode), where $\Delta G^\circ$ is the Gibbs free energy of the reaction and the redox potential $E^\circ_{ox}$ is $-\Delta G^\circ/nF$; $n$ is equal to 1 (number of electrons) and $F$ is the Faraday constant (96 485 C $mol^{-1}$).

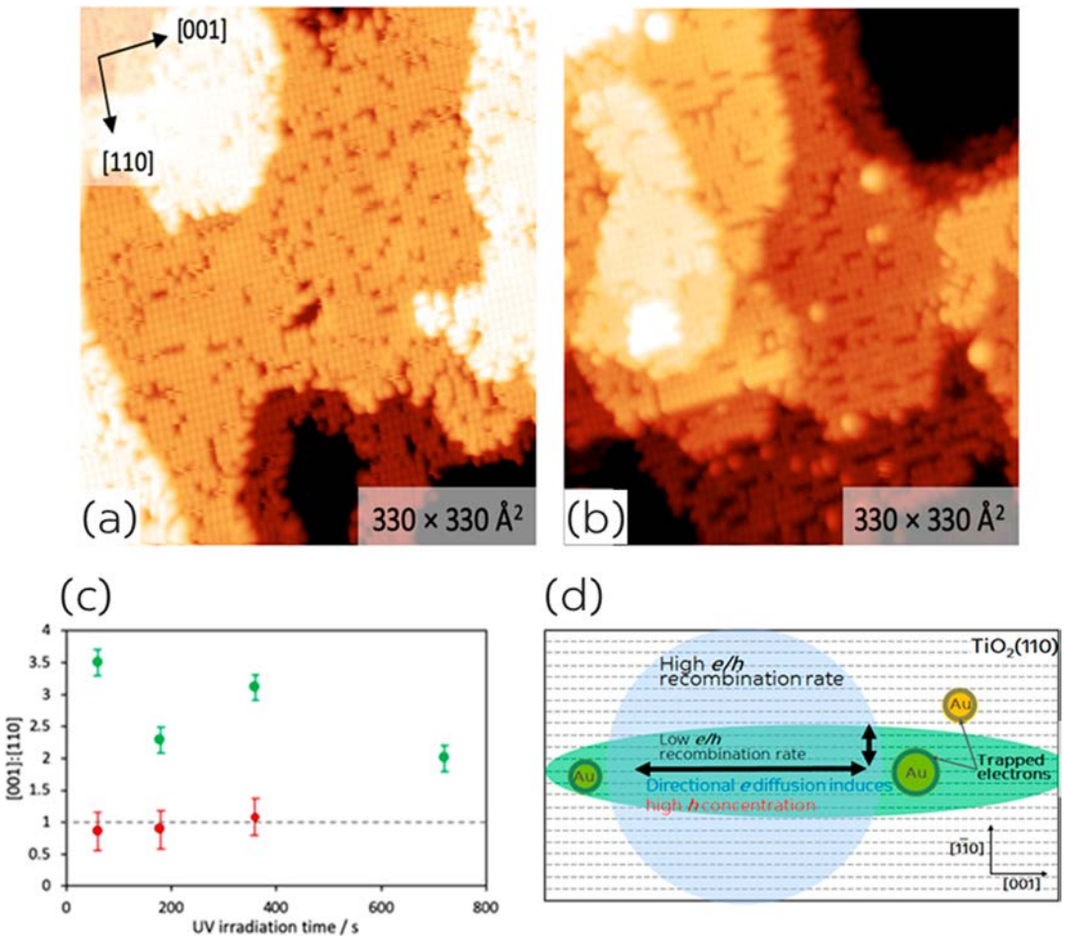


**Figure 7.** Images taken of benzoate overlayers (0.41 ML) following irradiation of $TiO_2$(110) and Au/$TiO_2$(110). (a) Bare benzoate covered (110) surface after 3 min of exposure to UV−vis light and (b) gold doped surface after 6 min of UV−vis irradiation (both images are recorded at a tip voltage $V_S$ = +2.0 V, $I_t$ = 0.03 nA). The choice of different time is to compare "reaction selectivity" at a similar "coverage". (c) Scatter plot comparing the direction of "chains" of empty benzoate sites at different irradiation times for the two surfaces, by recording the ratio of the number of chains along the [001] to those oriented along the [110]. There is a dotted line at [001]:[110] = 1, which indicates the value for an isotropic distribution. The values for the bare surface are plotted in red, and the gold loaded surface is in green. (d) Schematic representation of the excited electronic state upon light excitation. The green area represents a high hole concentration area, because electrons are preferentially diffusing along [001] and are trapped at Au clusters. The blue area is a representation of a domain that does not contain Au clusters and therefore will not have a preferential directional removal of benzoates. The length of black arrows represents the magnitude of electron conductivity along and perpendicular to the [001] direction. The dashed lines represent Ti cations, on top of which benzoates are formed. To compute for the anisotropic reaction displayed in (c), we have counted each instance of two or more adjacent molecular vacancies as a "chain", then compared the total number of chains in each direction, irrespective of length. Five images for each irradiation time were used, from which the average ratio is taken.

A distinct change in the orientation of these one dimen sional arrays of benzoate empty sites appears after irradiation when gold is present. Figure 7(c) compares the number of chains in the [001] direction to the number of chains in the [110] direction as a function of exposure time. A dotted line in Figure 7(c) superposed at [001]:[110] = 1 represents an equal distribution of the chain in both directions (i.e., isotropic or nondirectional coverage). In Figure 7(a), the bare benzoate layer has an equal number of chains in both directions, showing a lack of anisotropy. However, in the presence of Au clusters, we observed maximum 3.5 times higher chains oriented in the [001] direction (parallel to the $Ti_{5c}$ ions) than those along the [110] direction; see Figure 7(b). Lateral interaction of benzoate rings can have an attractive[65] (van der Waals) and repulsive (steric) nature.[66] Hence, removal of one adsorbate will affect the stability of adjacent molecules, which should occur in the presence or absence of Au clusters. This is, to our knowledge, the first time that anisotropy has been observed following a photoreaction of an organic molecule upon excitation of a metal/semiconductor system.

Anisotropic behavior has been observed at the atomic scale in the literature on metal oxides during mechanisms such as the deposition of metals to produce one dimensional nano wires[67] or the adsorption of molecules.[68,69] These behaviors are attributed to the anisotropic diffusion of adsorbates on the surfaces, aided by morphological and electronic structure effects. Although the anisotropic conductivity in rutile along [001] or the topographical landscape of the surface may play an important role in the underlying mechanism behind the creation of chains, they cannot adequately explain this anisotropic phenomenon.[70] If either were the sole driving physical mechanism, we would also see a preference in the orientation of the chains of empty sites on the bare benzoate layer. In the literature, DFT calculations found that the adsorption of benzoic acid causes a strong relaxation of subsurface layers of $TiO_2$(110), leading to disruption of the

Ti−O electronic hybridization.[71] One, however, would expect the hybridization to happen regardless of Au clusters.

A physical mechanism behind this anisotropic phenomenon is most likely due to the response of the complete electronic system as shown in Figure 7(d). For example, hybridization effects and its resulting band structures have explained the origins of photochemical anisotropy, observed for the selective reductive deposition of Ag ions on the $SrTiO_3(100)$.[72] On $TiO_2$, the diffusion of excited electrons has been studied experimentally and theoretically.[73,74] As reported, the diffusion of a hole is much slower than that of excited electrons; therefore, the former is expected to have the dominant role in an anisotropic phenomenon. The activation energy for the diffusion of a hole on the surface of $TiO_2(110)$ along the [001] direction is higher (0.62 eV) than that of excited electrons (0.40 eV);[75] holes are effectively $O^-$ anions (which are 2 or 3 fold coordinated to $Ti^{4+}$ cations along the [001] and [110] directions), while exited electrons are $Ti^{3+}$ cations (which are 5 or 6 fold coordinated to $O^{2-}$ anions). In the presence of Au clusters, excited electrons have a high chance of being trapped. Because the electron diffuses faster along the [001] direction than along the [110] direction, a preferential depletion can occur. The diffusion coefficient ($D_e$) of excited electrons is expressed as $R^2nk_{et}$,[73] where $R$ is the distance between two neighboring sites, $n$ is the number of neighboring electronic accepting sites, and $k_{et}$ is the adiabatic rate constant for the polaron electron transfer. $k_{et}$ has the form $\nu_n \exp(-\Delta G_{ad}^*/k_BT)$, with $\Delta G_{ad}^* = (1/4\ \lambda - V_{ii'})$, where $\nu_n$ is the frequency for nuclear motion, $\Delta G_{ad}^*$ is the adiabatic activation energy, $\lambda$ is the reorganization energy within the framework of Marcus theory, $V$ is the electronic coupling element, and ii′ are the positions of an excited electron at site i jumping into an empty site i′ ($D_e$ is ca. $10^{-5}$ $cm^2/s$).[71] On the $TiO_2(110)$, the distance between two Ti cations along the [001] direction is smaller than that along the [110] direction—2.96 Å compared to 6.5 Å—which partly explains the reason for the preferential diffusion; the shorter the distance, the smaller would be $\Delta G_{ad}^*$. A similar reasoning, based on bond distance, has been given to explain the directional charge diffusion in $V_2O_5$.[76] Equally important, molecular dynamics computation using DFT+U (3.9 eV) on the d orbitals of Ti cations indicated that a polaron on a Ti cation is preferentially located on $d_{yz}$ orbitals along the [001] direction and a non negligible (30%) hybridization exists with 2p orbitals of the in plane O anions.[77] These, taken together, may then contribute to the faster excited electron diffusion along this direction, which in turn leaves a larger concentration of holes along the [001] direction, amplified by their much slower diffusion rate. Because carboxylic acid reactions over excited $TiO_2$ are hole driven, they would preferentially react along the [001] direction, explaining the observed anisotropy during STM imaging.

## 5. CONCLUSIONS

STM results reveal that the adsorption of benzoic acid on Au/$TiO_2(110)$ causes the displacement of a large fraction of Au clusters from the terraces to the step edges. A complementary DFT+U study of benzoic acid/benzoate on s $TiO_2$, $Au_9$/s $TiO_2$, and $Au_9$/r $TiO_2$ indicates that this arises from the strong dissociative adsorption energy of benzoic acid (about −2.4 eV). This compares with the relatively small activation energy for Au cluster diffusion ($E_a$ of $Au_9$ = 0.38 eV) as well as the high activation energy for benzoates to diffuse on the surface ($E_a$ about 1.6 eV).

STM studies of light excited Au/$TiO_2(110)$, with Au nanoparticle diameters less than 10 Å, point to an anisotropic surface reaction of the organic adsorbate (benzoate species) from which a quantitative estimation of the anisotropy was conducted. Around a three times higher depletion rate along the [001] direction is observed in comparison to that found along the [110] direction. We postulate that this is linked to the already known anisotropic movement of excited electrons along the [001] direction. In the presence of Au clusters, these electrons may be trapped, leaving in turn a high concentrations of holes, thus increasing the reaction rate along this direction.

## AUTHOR INFORMATION


### Corresponding Authors

**Geoff Thornton** − *Department of Chemistry and London Centre for Nanotechnology (LCN), University College London (UCL), WC1H 0AH London, U.K.;* orcid.org/0000 0002 1616 5606; Email: g.thornton@ucl.ac.uk

**Hicham Idriss** − *Department of Chemistry and London Centre for Nanotechnology (LCN), University College London (UCL), WC1H 0AH London, U.K.; Surface Science and Advanced Characterisation, SABIC CRD at King Abdullah University for Science and Technology (KAUST), Thuwal 23955, Saudi Arabia;* Present Address: Institute of Functional Interfaces (IFG), Karlsruhe Institute of Technology (KIT), D 76344 Eggenstein Leopoldshafen, Germany; orcid.org/0000 0001 8614 7019; Email: h.idriss@ucl.ac.uk, hicham.idriss@kit.edu

### Authors

**Oscar Bentley Jerdmyr Williams** − *Department of Chemistry and London Centre for Nanotechnology (LCN), University College London (UCL), WC1H 0AH London, U.K.*

**Khabiboulakh Katsiev** − *Surface Science and Advanced Characterisation, SABIC CRD at King Abdullah University for Science and Technology (KAUST), Thuwal 23955, Saudi Arabia*

**Byeongjin Baek** − *SABIC Global Corporate Research, Sugar Land, Texas 77478, United States;* orcid.org/0000 0001 9314 828X

**George Harrison** − *KAUST Solar Center (KSC), Physical Sciences and Engineering Division (PSE), King Abdullah University for Science and Technology (KAUST), Thuwal 23955, Saudi Arabia*

## Author Contributions

[¶]O.B.J.W. and K.K. contributed equally.


## Funding

This work was supported by the European Research Council Advanced Grant ENERGYSURF and EPSRC (U.K.) (EP/L015277/1).


## Notes

The authors declare no competing financial interest.

## REFERENCES


(1) Idriss, H. The elusive photocatalytic water splitting reaction using sun light on suspended nanoparticles. Is there a way forward? *Catal. Sci. Technol.* **2020**, *10*, 304−310.

(2) Fujishima, A.; Honda, K. Electrochemical Photolysis of Water at a Semiconductor Electrode. *Nature* **1972**, *238*, 37−38.

(3) Stevanovic, A.; Büttner, M.; Zhang, Z.; Yates, J. T., Jr. Photoluminescence of $TiO_2$: Effect of UV Light and Adsorbed Molecules on Surface Band Structure. *J. Am. Chem. Soc.* **2012**, *134*, 324−332.

(4) Anpo, M.; Chiba, K.; Tomonari, M.; Coluccia, S.; Che, M.; Fox, M. A. Photocatalysis on Native and Platinum Loaded $TiO_2$ and ZnO Catalysts Origin of Different Reactivities on Wet and Dry Metal Oxides. *Bull. Chem. Soc. Jpn.* **1991**, *64*, 543−551.

(5) Berger, T.; Sterrer, M.; Diwald, O.; Knozinger, E.; Panayotov, D.; Thompson, T. L.; Yates, J. T., Jr Light Induced Charge Separation in Anatase $TiO_2$ Particles. *J. Phys. Chem. B* **2005**, *109*, 6061−6068.

(6) Plata, J. J.; Collico, V.; Márquez, A. M.; Sanz, J. F. Understanding Acetaldehyde Thermal Chemistry on the $TiO_2$ (110) Rutile Surface: From Adsorption to Reactivity. *J. Phys. Chem. C* **2011**, *115* (6), 2819−2825.

(7) Jayaweera, P. M.; Quah, E. L.; Idriss, H. Photoreaction of Ethanol on $TiO_2$(110) Single Crystal Surface. *J. Phys. Chem. C* **2007**, *111*, 1764−1769.

(8) Yu, Z.; Chuang, S. S. C. In situ IR study of adsorbed species and photogenerated electrons during photocatalytic oxidation of ethanol on $TiO_2$. *J. Catal.* **2007**, *246*, 118−126.

(9) Rismanchian, A.; Chen, Y. W.; Chuang, S. S. C. In situ infrared study of photoreaction of ethanol on Au and Ag/$TiO_2$. *Catal. Today* **2016**, *264*, 16−22.

(10) Hu, S.; Bopp, P. A.; Österlund, L.; Broqvist, P.; Hermansson, K. Formic Acid on $TiO_{2-x}$ (110): Dissociation, Motion, and Vacancy Healing. *J. Phys. Chem. C* **2014**, *118*, 14876−14887.

(11) Buchholz, M.; Xu, M.; Noei, H.; Weidler, P.; Nefedov, A.; Fink, K.; Wang, Y.; Wöll, C. Interaction of carboxylic acids with rutile $TiO_2$(110): IR investigations of terephthalic and benzoic acid adsorbed on a single crystal substrate. *Surf. Sci.* **2016**, *643*, 11−123.

(12) Nadeem, I. M.; Hargreaves, L.; Harrison, G. T.; Idriss, H.; Shluger, A. L.; Thornton, G. Carboxylate adsorption on rutile $TiO_2$ (100): role of Coulomb repulsion, relaxation, and steric hindrance. *J. Phys. Chem. C* **2021**, *125*, 13770−13779.

(13) Kim, K. S.; Barteau, M. A. Structure and Composition Requirements for Deoxygenation, Dehydration, and Ketonization Reactions of Carboxylic Acids on $TiO_2$(001) Single Crystal Surfaces. *J. Catal.* **1990**, *12*, 353−375.

(14) Titheridge, D. J.; Barteau, M. A.; Idriss, H. Reaction of Acrylic Acid on $TiO_2$(001) Single Crystal Surfaces. Evidence of Different Pathways for Vinyl and Carboxyl Groups. *Langmuir* **2001**, *17*, 2120−2128.

(15) Pang, C. L.; Lindsay, R.; Thornton, G. Structure of Clean and Adsorbate Covered Single Crystal Rutile $TiO_2$ Surfaces. *Chem. Rev.* **2013**, *113* (6), 3887−3948.

(16) Cosandey, F.; Madey, T. E. Growth, morphology, interfacial effects and catalytic properties of Au on $TiO_2$(110). *Surf. Rev. Lett.* **2001**, *8* (01n02), 73−93.

(17) Katsiev, K.; Harrison, G.; Thornton, G.; Idriss, H. Gold Cluster Coverage Effect on $H_2$ Production over Rutile $TiO_2$(110). *ACS Catal.* **2019**, *9*, 8294−8305.

(18) Vijay, A.; Mills, G.; Metiu, H. Adsorption of gold on stoichiometric and reduced rutile $TiO_2$ (110) surfaces. *J. Chem. Phys.* **2003**, *118*, 6536−6551.

(19) Pillay, D.; Wang, Y.; Hwang, G. S. A Comparative Theoretical Study of Au, Ag and Cu Adsorption on $TiO_2$(110) Rutile Surfaces. *Korean J. Chem. Eng.* **2004**, *21*, 537−547.

(20) Mellor, A.; Humphrey, D.; Yim, C. M.; Pang, C. L.; Idriss, H.; Thornton, G. Direct visualization of au atoms bound to $TiO_2$(110) O vacancies. *J. Phys. Chem. C* **2017**, *121*, 24721−24725.

(21) Thompson, T. L.; Yates, J. T., Jr. Control of a surface photochemical process by fractal electron transport across the surface: $O_2$ photodesorption from $TiO_2$(110). *J. Phys. Chem. B* **2006**, *110*, 7431−7435.

(22) Dai, X.; Jiao, Z.; Ma, Z.; Liu, K.; Wang, C.; Su, H. Capturing the Long Lived Photogenerated Electrons in Au/$TiO_2$ upon UV or Visible Irradiation by Time Resolved Infrared Spectroscopy. *J. Phys. Chem. C* **2019**, *123*, 20325−20332.

(23) Derkachova, A.; Kolwas, K.; Demchenko, I. Dielectric Function for Gold in Plasmonics Applications: Size Dependence of Plasmon Resonance Frequencies and Damping Rates for Nanospheres. *Plasmonics* **2016**, *11*, 941−951.

(24) Soldo Olivier, Y.; Abisset, A.; Bailly, A.; De Santis, M.; Garaudée, S.; Lacipière, J.; Coati, A.; Garreauc, Y.; Saint Lager, M. C. Localized surface plasmon resonance of Au/$TiO_2$(110): substrate and size influence from in situ optical and structural investigation. *Nanoscale Adv.* **2020**, *2*, 2448−2461.

(25) Maity, P.; Katsiev, K.; Mohammed, O. F.; Idriss, H. Bulk Defect Mediated Photoexcited Charge Recombination in Anatase and Rutile $TiO_2$ Single Crystals. *J. Phys. Chem. C* **2018**, *122*, 8925−8932.

(26) Hollander, L. E., Jr.; Castro, P. L. Anisotropic Conduction in Nonstoichiometric Rutile ($TiO_2$). *Phys. Rev.* **1960**, *119*, 1882−1885.

(27) Byl, O.; Yates, J. T., Jr. Anisotropy in the Electrical Conductivity of Rutile $TiO_2$ in the (110) Plane. *J. Phys. Chem. B* **2006**, *110*, 22966−22967.

(28) Solanki, V.; Joshi, S. R.; Mishra, I.; Kanjilal, D.; Varma, S. Formation of Anisotropic Nanostructures on Rutile $TiO_2$(110) Surfaces and Their Photo Absorption Properties. *Metallurgical and materials transactions A* **2018**, *49A*, 3117−3121.

(29) Henderson, M. A.; White, J. M.; Uetsuka, H.; Onishi, H. Selectivity changes during organic photooxidation on $TiO_2$: Role of $O_2$ pressure and organic coverage. *J. Catal.* **2006**, *238*, 153−164.

(30) Du, Y.; Petrik, N. G.; Deskins, N. A.; Wang, Z.; Henderson, M. A.; Kimmel, G. A.; Lyubinetsky, I. Hydrogen reactivity on highly hydroxylated $TiO_2$(110) surfaces prepared via carboxylic acid adsorption and photolysis. *Phys. Chem. Chem. Phys.* **2012**, *14*, 3066−3074.

(31) Wilson, J. N.; Idriss, H. Structure Sensitivity and Photocatalytic Reactions of Semiconductors. Effect of the Last Layer Atomic Arrangement. *J. Am. Chem. Soc.* **2002**, *124*, 11284−11285.

(32) Idriss, H.; Légaré, P. G.; Maire, G. Dark and photoreactions of acetates on TiO2() single crystal surface. *Surf. Sci.* **2002**, *515*, 413−420.

(33) Quah, E. L.; Wilson, J. N.; Idriss, H. Photoreaction of Acetic Acid on Rutile $TiO_2$ (011) single crystal surface. *Langmuir* **2010**, *26*, 6411−6417.

(34) Sandell, A.; Ragazzon, D.; Chaefer, A.; Farstad, M. H.; Borg, A. Photochemistry of Carboxylate on $TiO_2$(110) Studied with Synchrotron Radiation Photoelectron Spectroscopy. *Langmuir* **2016**, *32*, 11456−11464.

(35) Xia, Y.; Zhu, K.; Zhang, Z.; Park, K. Photo stimulated desorption of trimethyl acetic acid on cross linked (1 × 2) $TiO_2$ (110) probed by scanning tunneling microscopy. *Appl. Surf. Sci.* **2020**, *511*, 145553.

(36) Zhang, Z.; Bondarchuk, O.; Kay, B. D.; White, J. M.; Dohnálek, Z. Imaging Water Dissociation on $TiO_2$(110): Evidence for Inequivalent Geminate OH Groups. *J. Phys. Chem. C* **2008**, *112*, 9006−9015.

(37) Matthey, D.; Wang, J. G.; Wendt, S.; Matthiesen, J.; Schaub, R.; Laegsgaard, E.; Hammer, B.; Besenbacher, F. Enhanced bonding of

gold nanoparticles on oxidized $TiO_2$(110). *Science* **2007**, *315*, 1692−1696.
(38) Kresse, G.; Hafner, J. Ab Initio Molecular Dynamics Simulation of the Liquid Metal Amorphous Semiconductor Transition in Ger manium. *Phys. Rev. B* **1994**, *49*, 251−269.
(39) Kresse, G.; Hafner, J. Ab Initio Molecular Dynamics for Liquid Metals. *Phys. Rev. B* **1993**, *47*, 558−561.
(40) Kresse, G.; Furthmüller, J. Efficiency of Ab Initio Total Energy Calculations for Metals and Semiconductors Using a Plane Wave Basis Set. *Comput. Mater. Sci.* **1996**, *6*, 15−50.
(41) Wellendorff, J.; Lundgaard, K. T.; Møgelhøj, A.; Petzold, V.; Landis, D. D.; Nørskov, J. K.; Bligaard, T.; Jacobsen, K. W. Density Functionals for Surface Science: Exchange Correlation Model Development with Bayesian Error Estimation. *Phys. Rev. B* **2012**, *85*, 235149.
(42) Perdew, J. P.; Burke, K.; Ernzerhof, M. Generalized Gradient Approximation Made Simple. *Phys. Rev. Lett.* **1996**, *77*, 3865−3868.
(43) Bahn, S. R.; Jacobsen, K. W. An Object Oriented Scripting Interface to a Legacy Electronic Structure Code. *Comput. Sci. Eng.* **2002**, *4*, 56−66.
(44) Dudarev, S.; Botton, G. Electron Energy Loss Spectra and the Structural Stability of Nickel Oxide: An LSDA+ U Study. *Phys. Rev. B* **1998**, *57*, 1505−1509.
(45) Yoo, S.; Siemer, N.; Todorova, M.; Marx, D. Deciphering Charge Transfer and Electronic Polarization E Ff Ects at Gold Nanocatalysts on Reduced Titania Support. *J. Phys. Chem. C* **2019**, *123*, 5495−5506.
(46) Monkhorst, H. J.; Pack, J. D. Special Points for Brillouin Zone Integrations. *Phys. Rev. B* **1976**, *13*, 5188−5192.
(47) Chueh, Y. L.; Hsieh, C. H.; Chang, M. T.; Chou, L. J.; Lao, C. S.; Song, J. H.; Gan, J. Y.; Wang, Z. L. RuO2 Nanowires and $RuO_2$/$TiO_2$ Core/Shell Nanowires: From Synthesis to Mechanical, Optical, Electrical, and Photoconductive Properties. *Adv. Mater.* **2007**, *19*, 143−149.
(48) Henkelman, G.; Uberuaga, B. P.; Jónsson, H. A Climbing Image Nudged Elastic Band Method for Finding Saddle Points and Minimum Energy Paths. *J. Chem. Phys.* **2000**, *113*, 9901−9904.
(49) Teobaldi, G.; Hofer, W. A.; Bikondoa, O.; Pang, C. L.; Cabailh, G.; Thornton, G. Modelling STM images of $TiO_2$(110) from first principles: Defects, water adsorption and dissociation products. *Phys. Rev. Lett.* **2007**, *437*, 73−78.
(50) Sánchez Sánchez, C.; González, C.; Jelinek, P.; Méndez, J.; de Andres, P. L.; Martín Gago, J. A.; López, M. F. Understanding atomic resolved STM images on $TiO_2$(110) (1 × 1) surface by DFT calculations. *Nanotechnology* **2010**, *21*, 405702.
(51) Skibinski, E. S.; Song, A.; De Benedetti, W. J. I.; Ortoll Bloch, A. G.; Hines, M. A. Solution Deposition of Self Assembled Benzoate Monolayers on Rutile (110): Effect of $\pi-\pi$ Interactions on Monolayer Structure. *J. Phys. Chem. C* **2016**, *120*, 11581−11589.
(52) Grinter, D. C.; Woolcot, T.; Pang, C. L.; Thornton, G. Ordered Carboxylates on $TiO_2$(110) Formed at Aqueous Interfaces. *J. Phys. Chem. Lett.* **2014**, *5*, 4265−4269.
(53) Busayaporn, W.; Duncan, D. A.; Allegretti, F.; Wander, A.; Bech, M.; Møller, P. J.; Doyle, B. P.; Harrison, N. M.; Thornton, G.; Lindsay, R. Structure of a Model Dye/Titania Interface: Geometry of Benzoate on Rutile $TiO_2$ (110)(1 × 1). *J. Phys. Chem. C* **2016**, *120*, 14690−14698.
(54) Onishi, H.; Fukui, K. i; Iwasawa, Y. Space Correlation Analysis of Formate Ions Adsorbed on $TiO_2$ (110). *Jpn. J. Appl. Phys.* **1999**, *38*, 3830−3832.
(55) Kolmakov, A.; Goodman, D. W. In situ scanning tunneling microscopy of oxide supported metal clusters: Nucleation, growth, and thermal evolution of individual particles. *Chem. Rec.* **2002**, *2*, 446−457.
(56) Koga, H. Conference ISSS 7 DFT Study of CO Oxidation Catalyzed by Au/$TiO_2$ : Activity of Small Clusters. *e Journal Surf. Sci. Nanotechnol.* **2015**, *13*, 129−134.
(57) Wahlström, E.; Lopez, N.; Schaub, R.; Thostrup, P.; Rønnau, A.; Africh, C.; Laegsgaard, E.; Nørskov, J. K.; Besenbacher, F. Bonding of Gold Nanoclusters to Oxygen Vacancies on Rutile $TiO_2$(110). *Phys. Rev. Lett.* **2003**, *90*, 1−4.
(58) Yim, C. M.; Lamoureux, P. S.; Mellor, A.; Pang, C. L.; Idriss, H.; Pacchioni, G.; Thornton, G. Size and Shape Dependence of the Electronic Structure of Gold Nanoclusters on $TiO_2$. *J. Phys. Chem. Lett.* **2021**, *12*, 8363−8369.
(59) Tosoni, S.; Pacchioni, G. Trends in Adhesion Energies of Gold on MgO (100), Rutile $TiO_2$ (110), and $CeO_2$ (111) Surfaces : A Comparative DFT Study. *J. Phys. Chem. C* **2017**, *2*, 28328−28338.
(60) Li, L.; Yi Gao, Y.; Li, H.; Zhao, Y.; Pei, Y.; Chen, Z.; Zeng, X. C. CO Oxidation on $TiO_2$ (110) Supported Subnanometer Gold Clusters: Size and Shape Effects. *J. Am. Chem. Soc.* **2013**, *2* (2013), 19336−19346.
(61) Liu, N.; Yin, P.; Xu, M.; Yang, Y.; Zhang, S.; Zhang, J.; Meng, X.; Zhang, J.; Yu, J.; Man, Y.; Zhang, X.; Wei, M. The catalytic mechanism of the Au@$TiO_{2-x}$/ZnO catalyst towards a low temper ature water gas shift reaction. *Catal. Sci. Technol.* **2020**, *10*, 768−775.
(62) Li, L.; Li, W.; Zhu, C.; Mao, L. F. A DFT+U study about agglomeration of Au atoms on reduced surface of rutile $TiO_2$ (110). *Mater. Chem. Phys.* **2021**, *271*, 124944.
(63) Iddir, H.; Öğüt, S.; Browning, N. D.; Disko, M. M. Adsorption and diffusion of Pt and Au on the stoichiometric and reduced $TiO_2$ rutile (110) surfaces. *Phys. Rev. B* **2005**, *72*, 81407.
(64) Landis, E. C.; Jensen, S. C.; Phillips, K. R.; Friend, C. M. Photostability and Thermal Decomposition of Benzoic Acid on $TiO_2$. *J. Phys. Chem. C* **2012**, *116*, 21508−21513. Henderson, M. A. Acetone Chemistry on Oxidized and Reduced $TiO_2$(110). *J. Phys. Chem. B* **2004**, *108*, 18932−18941.
(65) Buchholz, M.; Xu, M.; Noei, H.; Weidler, P.; Nefedov, A.; Fink, K.; Wang, Y.; Wöll, C. Interaction of carboxylic acids with rutile $TiO_2$(110): IR investigations of terephthalic and benzoic acid adsorbed on a single crystal substrate. *Surf. Sci.* **2106**, *643*, 117−123.
(66) Heckel, W.; Würger, T.; Müller, S.; Feldbauer, G. Van der Waals Interaction Really Matters: Energetics of Benzoic Acid on $TiO_2$ Rutile Surfaces. *J. Phys. Chem. C* **2017**, *121*, 17207−17214.
(67) Katsiev, K.; Batzill, M.; Diebold, U.; Urban, A.; Meyer, B. Growth of One Dimensional Pd Nanowires on the Terraces of a Reduced $SnO_2$(101) Surface. *Phys. Rev. Lett.* **2007**, *98*, 186102.
(68) He, Y.; Li, W. K.; Gong, X. Q.; Dulub, O.; Selloni, A.; Diebold, U. Nucleation and Growth of 1D Water Clusters on Rutile $TiO_2$(011) 2 × 1. *J. Phys. Chem. C* **2009**, *113*, 10329−10332.
(69) Kimmel, G. A.; Baer, M.; Petrik, N. G.; VandeVondele, J.; Rousseau, R.; Mundy, C. J. Polarization and Azimuth Resolved Infrared Spectroscopy of Water on $TiO_2$(110): Anisotropy and the Hydrogen Bonding Network. *J. Phys. Chem. Lett.* **2012**, *4* (1), 53−57.
(70) Byl, O.; Yates, J. T. Anisotropy in the Electrical Conductivity of Rutile $TiO_2$ in the (110) Plane. *J. Phys. Chem. B* **2006**, *110*, 22966−22967.
(71) Martsinovich, N.; Jones, D. R.; Troisi, A. Electronic Structure of $TiO_2$ Surfaces and Effect of Molecular Adsorbates Using Different DFT Implementations. *J. Phys. Chem. C* **2010**, *114*, 22659−22670.
(72) Giocondi, J. L.; Salvador, P. A.; Rohrer, G. S. The origin of photochemical anisotropy in $SrTiO_3$. *Top. Catal.* **2007**, *44*, 529−533.
(73) Duzhko, V.; Timoshenko, V. Yu.; Koch, F.; Dittrich, Th. Photovoltage in nanocrystalline porous $TiO_2$. *Phys. Rev. B* **2001**, *64* (1−7), 07520.
(74) Deskins, N. A.; Dupuis, M. Electron transport via polaron hopping in bulk $TiO_2$: A density functional theory characterization. *Phys. Rev. B* **2007**, *75* (1−10), 195212.
(75) Deskins, N. A.; Dupuis, M. Intrinsic Hole Migration Rates in $TiO_2$ from Density Functional Theory. *J. Phys. Chem. C* **2009**, *113*, 346−358.
(76) Watthaisong, P.; Ungthawan, S.; Pussana Hirunsit, P.; Suthirakun, S. Transport properties of electron small polarons in a $V_2O_5$ cathode of Li ion batteries: a computational study. *RSC Adv.* **2019**, *9*, 19483−19494.
(77) Reticcioli, M.; Setvin, M.; Schmid, M.; Diebold, U.; Franchini, C. Formation and dynamics of small polarons on the rutile $TiO_2$(110) surface. *Phys. Rev. B* **2018**, *98* (1−14), 045306.

Karlsruher Institut für Technologie

OPEN ACCESS

# Repository KITopen

Dies ist ein Postprint/begutachtetes Manuskript.

Empfohlene Zitierung:

Williams, O. B. J.; Katsiev, K.; Baek, B.; Harrison, G.; Thornton, G.; Idriss, H.
Direct Visualization of a Gold Nanoparticle Electron Trapping Effect
2022. Journal of the American Chemical Society, 144.
doi:10.5445/IR/1000146286

Zitierung der Originalveröffentlichung:

Williams, O. B. J.; Katsiev, K.; Baek, B.; Harrison, G.; Thornton, G.; Idriss, H.
Direct Visualization of a Gold Nanoparticle Electron Trapping Effect
2022. Journal of the American Chemical Society, 144 (2), 1034–1044.
doi:10.1021/jacs.1c12197

**Lizenzinformationen: KITopen-Lizenz**